Inorganic Chemistry Communications 160 (2024) 111920

Contents lists available at ScienceDirect

Inorganic Chemistry Communications

journal homepage: www.elsevier.com/locate/inoche

Short communication

Rare earth Gd^{3+} substituted on cobalt ferrites: Structural and dielectric studies by citrate gel autocombustion method

K. Vani [a], N. Hari kumar [b], D. Ravinder [a,*]

[a] University College of Science, Department of Physics, Osmania University, Telangana 500007, Hyderabad, India
[b] Department of Physics, St.Mary 's Group of Institutions, Deshmukhi, Yadadri Bhongiri 508116,India

ARTICLE INFO

Keywords:
Spinel ferrites
Structura studies
Dielectric studies
Applications

ABSTRACT

Gadolinium-doped cobalt ferrite ($CoGd_xFe_{2-x}O_4$; X = 0–0.025 in a 0.005 interval) was synthesised using citrate gel autocombustion. The effect of Gd^{3+} ions on structural, dielectric, and magnetic characteristics has been investigated. X-ray diffraction (XRD), scanning electron microscopy (SEM), Fourier transform infrared (FTIR) spectroscopy, ultraviolet visible spectroscopy (UV), an impedance (dielectric) analyzer, and a vibrating sample magnetometer (VSM) were used to characterise the as-synthesised materials. X-ray diffraction powder patterns were used to confirm phase identification and spinel structure, and the Williamson-Hall plot was used to investigate the crystalline size and lattice strain on the peak broadening of each sample, with crystalline size ranging from 13 to 48 nm. The scanning electron microscopy (SEM) micrographs demonstrate particle agglomeration, while energy dispersive spectroscopy (EDAX) pictures indicate the purity and existence of all elements in the created material samples. The frequency-dependent dielectric constant, dielectric loss, and AC electrical conductivity in the frequency range 50 Hz–1 MHz. The behaviour of dielectric properties has been studied using the Maxwell-Wagner model and Koop's theory. Because of this, higher frequencies show less dielectric loss, making them appropriate for use in high-frequency device applications.

1. Introduction

Due to their unique combination of electric and magnetic properties, spinel ferrites are very significant magnetic materials. The aforementioned characteristics render spinel ferrites advantageous in an extensive array of technological contexts, such as high-density magnetic recording, magnetic bioseparation, drug delivery, magnetic resonance imaging, high-frequency applications, microwave devices, electric insulators, memory cores, and hyperthermia. The basic electrical and magnetic properties can be adjusted depending on the application [1]. Spinel ferrites have the chemical formula MFe_2O_4 (where M is Ni, Co, Zn, etc.), in which Fe occupies the octahedral (B) site and M occupies the tetrahedral (A) site, and oxygen anions form a face-centred cubic structure that is tightly packed [2,3]. The unique electrical, optical, and magnetic properties of cobalt-based spinel ferrites ($CoFe_2O_4$), which crystallise in inverse spinel structure in bulk materials and spinel cubic structure with space group Fd-3 m in nanoparticles, are of great interest. These properties include a high Curie temperature, moderate saturation magnetization, large magnetocrystalline anisotropy, a large magnetostrictive coefficient, excellent chemical stability, and good thermal stability. The synthesis method can significantly affect the physical and chemical characteristics of cobalt ferrites by substituting different cations at tetrahedral or octahedral locations. Studying electrical conductivity and dielectric characteristics yields important insights into the actions of localised electron charge carriers, which can lead to increased knowledge of the dielectric polarisation mechanism in the ferrite under investigation [4,5]. As a result, rare earth lanthanides and gadolinium are commonly used to adjust the properties of cobalt ferrites in order to improve their remarkable qualities because they are very good electrical insulators with high resistance [6,7]. M. Hasim et al. conducted research on the substitution of RE = Ce and Dy on cobalt ferrites, which demonstrated that increasing the Ce and Dy concentrations increases coercivity while decreasing magnetization values [8]. C. Murugesan et al. substituted Gd on cobalt ferrites and found that the dielectric constant increases as Gd concentration increases [9]. Aravind Kumar et al. synthesised Gd-substituted cobalt ferrites and discovered that the dielectric constant decreases as Gd concentration and frequency increase [10]. Erum Pervaiz et al. prepared Gd-doped cobalt ferrites and reported that room-temperature DC electric resistivity increases to $9.5x10^7$ with Gd concentration except for x = 0.025 ($\sim 10^6$), and that

* Corresponding author.
E-mail addresses: ravindergupta29@rediffmail.com, aknhkou@gmail.com (D. Ravinder).

https://doi.org/10.1016/j.inoche.2023.111920
Received 21 October 2023; Received in revised form 16 November 2023; Accepted 12 December 2023
Available online 13 December 2023
1387-7003/Published by Elsevier B.V.

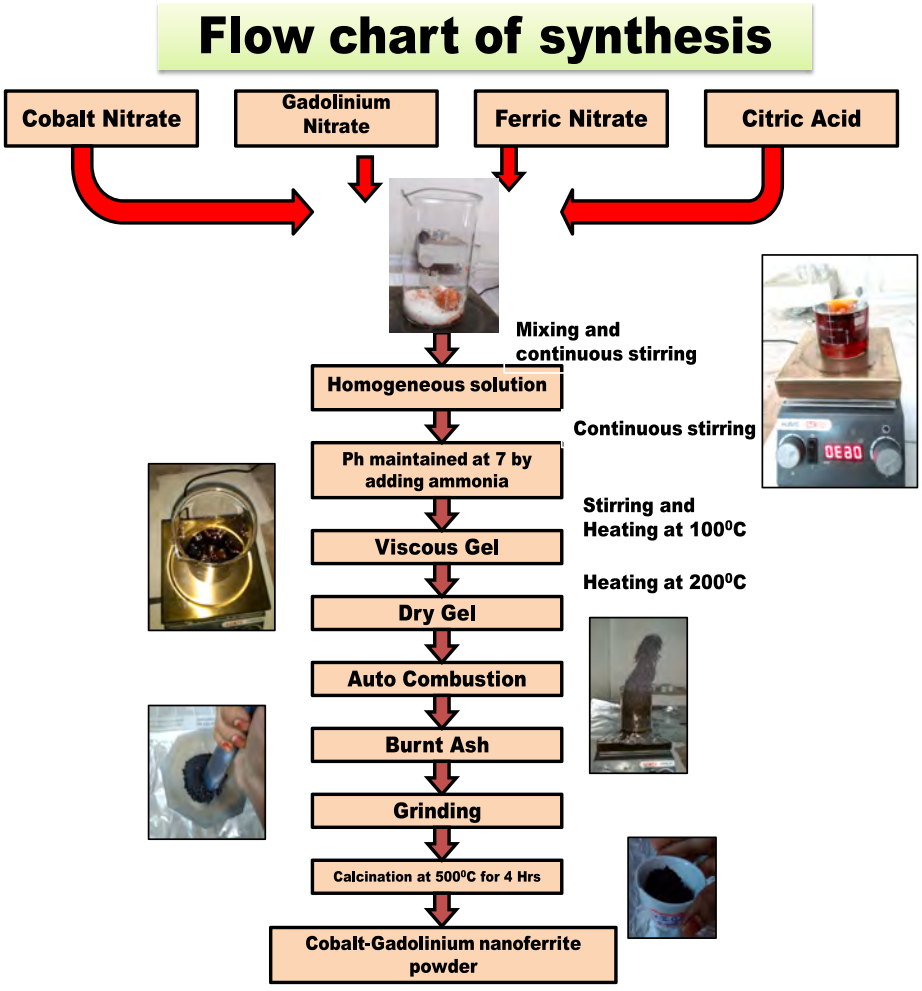

Fig. 1. Flow chart of $CoGd_xFe_{2-x}O_4$ nanoferrites.

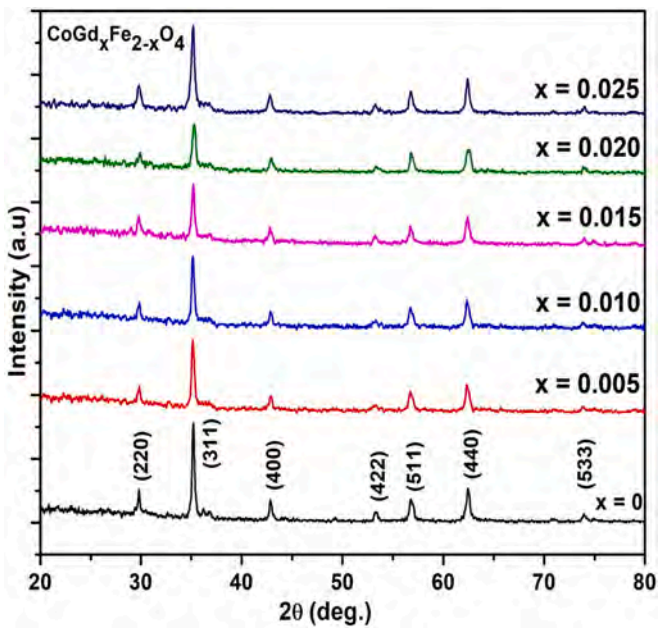

Fig. 2. XRD powder patterns of $CoGd_xFe_{2-x}O_4$ (x = 0–0.025 in an interval of 0.005) nanoferrites.

dielectric constant and dielectric loss decrease to 4.9 and 0.016, respectively, with increased dopant concentration and soft magnetic behaviour due to Gd substitution [11]. M. Kamran et al. developed La-doped cobalt ferrites and observed that increasing La doping reduces dielectric constants, dielectric losses, and AC conductivity values, while increasing La concentration increases DC electric resistivity [12]. L. Avazpour developed Eu and Nd-doped cobalt ferrites and discovered that at room temperature, the saturation magnetization of the ferrite ceramics decreases with grain size [13].

A simple auto-combustion method employing citric acid as the combustion agent was used to create samples of cobalt ferrite nanopowder doped with gadolinium (Gd). Cobalt ferrite nanopowder activity is greatly increased by the correlation between the agreement between XRD and SEM, which is addressed. High frequency variation discourse: its dielectric characteristics. The substitution of a small amount of gadolinium ions into cobalt ferrites was proposed to improve the synthesis, structural and dielectric properties.

2. Sample preparation

A citrate-gel autocombustion method was used to create gadolinium-substituted cobalt ferrites with the chemical formula CGF with X = 0, 0.005, 0.010, 0.015, 0.020, and 0.025. As reactants in the first step, cobalt nitrate (Co-95.6 mol%), ferric nitrate (Fe-25 mol%), gadolinium nitrate (Gd-99.8 mol%), and citric nitrate analytical grade are employed. The required amount of reactants is weighted, and the molar ratio of metal nitrate to citric acid is 1:3. Weighted metal nitrates and

Table 1
Crystallite size, Cell parameter, volume, X-ray density, hopping lengths(L_A & L_B) and strain for $CoGd_xFe_{2-x}O_4$ (x = 0–0.025 in an interval of 0.005) nanoferrites.

Samples	Average crystallite size, D(nm)	Cell parameter a(Å)	Volume of unit cell, V a = b = c (Å^3)	X-ray density, d_x(gm/cm^3)	Hopping length for site A, L_A (Å)	Hopping length for site B, L_B (Å)	Strain (ε)
$CoFe_2O_4$	48.2721	8.452	603.9	5.160	3.6601	2.9885	0.0015
$CoGd_{0.005}Fe_{1.995}O_4$	34.6450	8.459	605.3	5.159	3.6630	2.9908	0.00167
$CoGd_{0.010}Fe_{1.990}O_4$	31.0764	8.460	605.5	5.169	3.6633	2.9911	0.00268
$CoGd_{0.015}Fe_{1.985}O_4$	24.0159	8.457	604.9	5.185	3.6621	2.9901	0.00565
$CoGd_{0.020}Fe_{1.980}O_4$	22.9139	8.429	599.0	5.247	3.6502	2.9804	0.00672
$CoGd_{0.025}Fe_{1.975}O_4$	13.0113	8.458	605.2	5.205	3.6628	2.9906	−0.00105

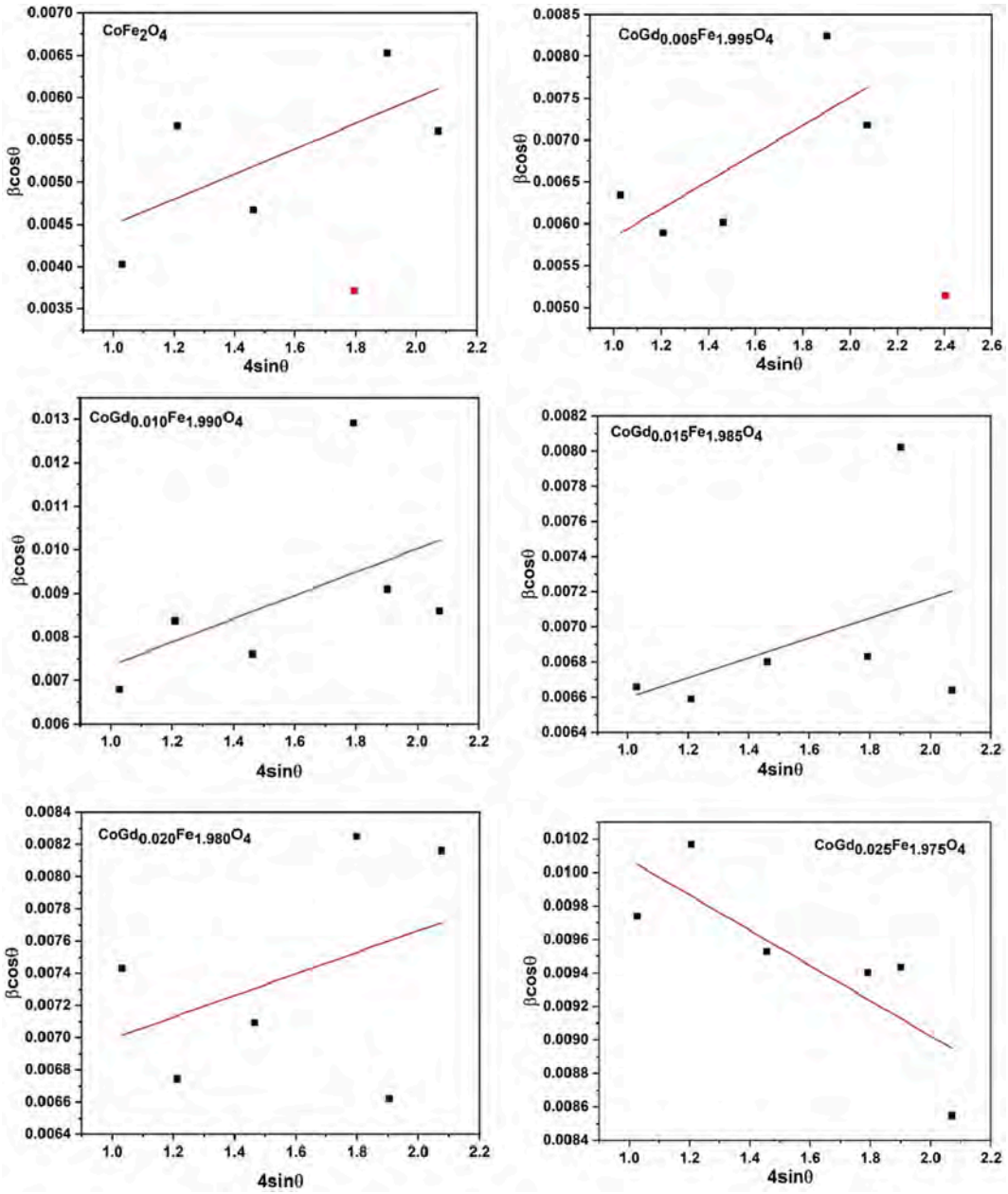

Fig. 3. W-H plots of $CoGd_xFe_{2-x}O_4$ (x = 0–0.025 in an interval of 0.005) nanoferrites.

citric acid are dissolved in deionized water and stirred together using a magnetic stirrer to create a homogenous solution [14]. The pH of the solution is adjusted to 7 by adding 25 % ammonia solution while continuously stirring. The resultant nitrate-citrate solution is allowed to condense by heating it on a hot plate of a magnetic stirrer at roughly 100 °C until it forms a highly viscous and dry gel. The dried gel is then heated on a hot plate at 200 °C until it self-ignites, resulting in auto-combustion. The end result is CoGd nanopowder. The nanopowders were pounded in an agate motor and pestle for 2–3 h to produce a fine powder, which was then heat treated in air at 500 degrees celsius for 4 h. Calcinated powders were combined with PVA binder and crushed at 5 tonnes in a hydraulic press to make pellets (13 mm in diameter), which

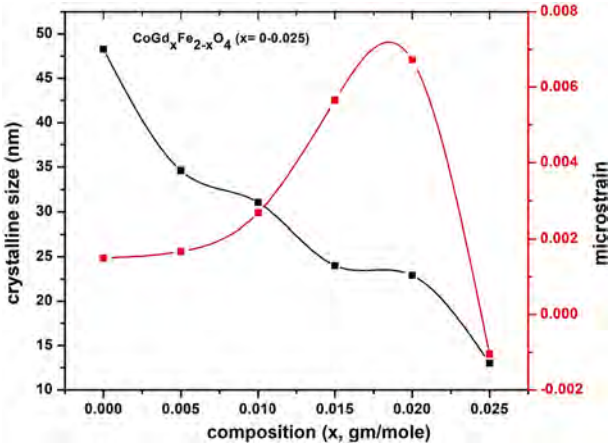

Fig. 4. Variation of crystalline size and micro strain with respect to composition of $CoGd_xFe_{2-x}O_4$ (x = 0–0.025 in an interval of 0.005) ferrites.

were then sintered at 500 °C for 4 h [15]. They are then dispatched to be characterised using various techniques. The synthesis flow chart is shown in Fig. 1.

3. Results and discussion

3.1. XRD analysis

Figure 2 depicts the X-ray diffraction patterns of CGF (x = 0–0.025 in an interval of 0.005) ferrites at room temperature, with a well-defined Bragg's reflection detected for the strongest peak with no impurity phases. The diffraction peaks observed at two correspond to the planes at (220), (311), (400), (422), (511), (440), and (533) for the most intense peaks at 30.1°, 35.5°, 43.1°, 53.5°, 57.0°, 62.6°, 74.1°. This confirmed the formation of spinel-structure cubic cobalt nanoferrites within the space group of Fd 3 m with JCPDS Card No. 22–1086 [16]. Furthermore, no new intensity peak is seen in the XRD pattern following Gd doping in cobalt nanoferrites. XRD examination verified that all of the products had single-phase crystalline structures [17–19].

The structural parameters lattice constant (a), unit cell volume (V), crystallite size (D), and X-ray density (dx) were computed using the following formulas (1–5) and are presented in Table 1.

$$a = d\sqrt{h^2 + k^2 + l^2}$$

where d is the inter-planar spacing, (h k l) are the miller indices.

$$V = a^3 \tag{2}$$

here 'a' is lattice constant,

$$D = \frac{K\lambda}{\beta cos\theta} \tag{3}$$

From the Debye-Scherer's formula [20], where K is a dimensionless shape factor having a value between 0.9 and 1, is a diffractometer with an X-ray wavelength (CuK_α source, i.e., λ = 1.5406 Å), β is the line broadening at full width at half-maximum of each phase (in radians), and θ is the Bragg angle (in degrees), is used to calculate these quantities.

$$dx = \frac{8M}{VN} \tag{4}$$

where M is the molecular weight of the sample, V is the volume of the unit cell, N is Avogadro's number ($6.023x10^{23}$).

For ferrites, the hopping lengths L, i.e., the distance between the magnetic ions, affect the physical properties, as reported by various authors. The hopping lengths of sites A and B, represented by L_A and L_B, were calculated using the equations.

$$L_A = \frac{a\sqrt{3}}{4}\text{Å} \text{ and } L_B = \frac{a\sqrt{2}}{4}\text{Å} \tag{5}$$

where a is the lattice parameter.

When Gd is incorporated into cobalt ferrite, the cell parameter (a) value increases due to the difference in the ionic radii of Gd^{3+} (1.107), which is bigger than the ionic radii of Fe^{3+} (0.76) [18]. Series $CoGd_xFe_{2-x}O_4$ crystallite sizes were determined to be 48.27, 34.64, 31.07, 24.01, 22.91, and 13.01 nm (x = 0, 0.005, 0.010, 0.015, 0.020, 0.025) and decreased with increasing Gd concentration. Actual broadening β_{in}^2 of diffraction peaks is corrected for experimental (β_{ex}) instrumental widening as $\beta = \beta_{ex}^2 - \beta_{in}^2$. Taking into account the size and strain effects, the Williamson-Hall equation for actual broadening β_{in}^2 can be modelled as follows:

$$\beta = \frac{K\lambda}{Dcos\theta} + 4\varepsilon tan\theta \tag{6}$$

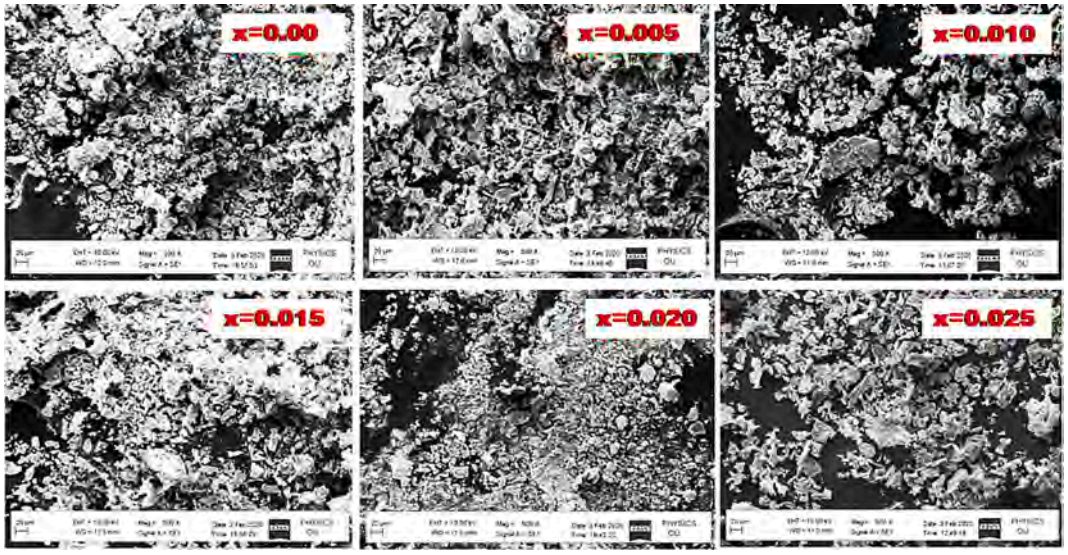

Fig. 5. SEM micrographs of $CoGd_xFe_{2-x}O_4$ (x = 0.0–0.025) nanoferrites.

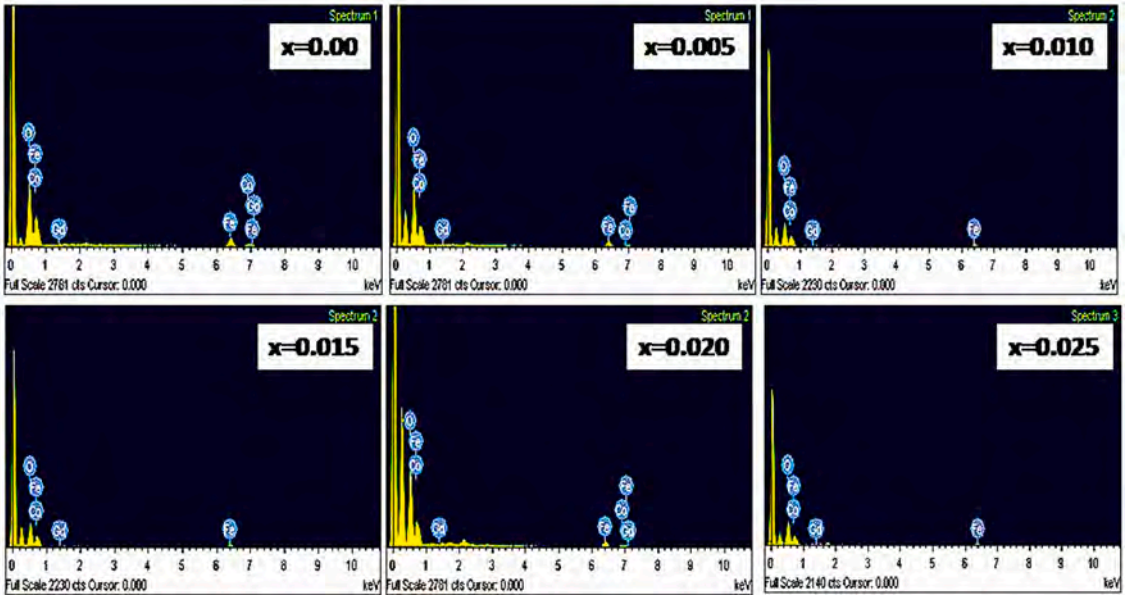

Fig. 6. EDAX images of $CoGd_xFe_{2-x}O_4$ (x = 0–0.025 in an interval of 0.005) nanoferrites.

Table 2
EDAX structure of $CoGd_xFe_{2-x}O_4$ (x = 0.0–0.025) nanoferrites.

x	Weight % of elements				Atomic % of elements			
	Co	Fe	Gd	O	Co	Fe	Gd	O
0.00	29.28	46.15	–	24.57	16.87	29.01	–	53.92
0.005	28.20	41.83	1.53	28.44	15.87	24.84	0.32	58.96
0.010	29.56	41.57	1.17	27.71	16.80	24.94	0.25	58.01
0.015	30.56	43.16	2.18	24.10	18.44	27.49	0.49	53.58
0.020	24.76	36.56	7.45	31.22	13.67	21.30	1.54	63.49
0.025	27.39	42.30	5.28	25.03	16.48	26.86	1.19	55.47

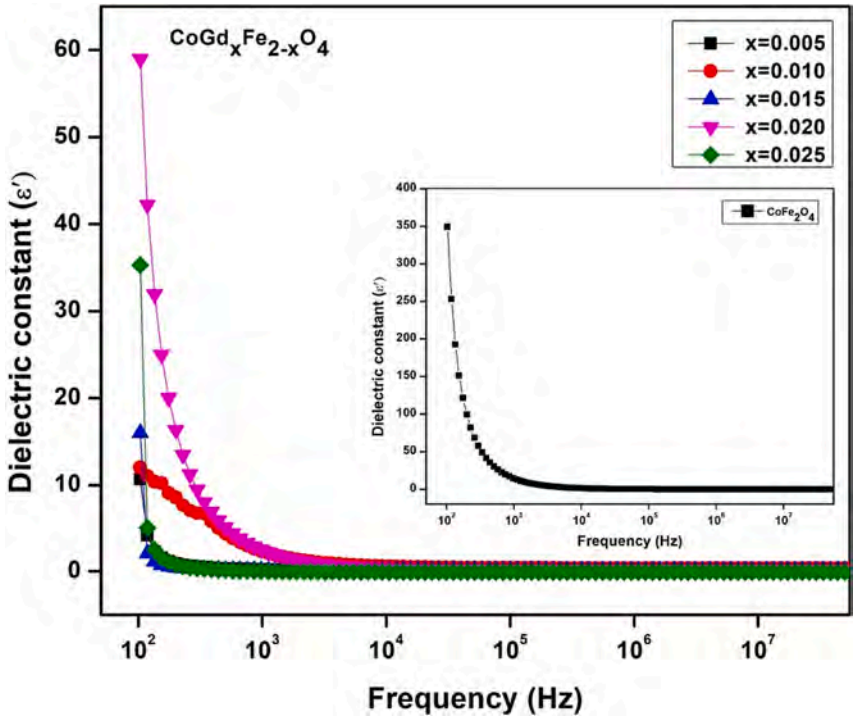

Fig. 7. Variation of Dielectric constant (ε′) of $CoGd_xFe_{2-x}O_4$ (x = 0–0.025 in an interval of 0.005) nanoferrites as a function of frequency at room temperature.

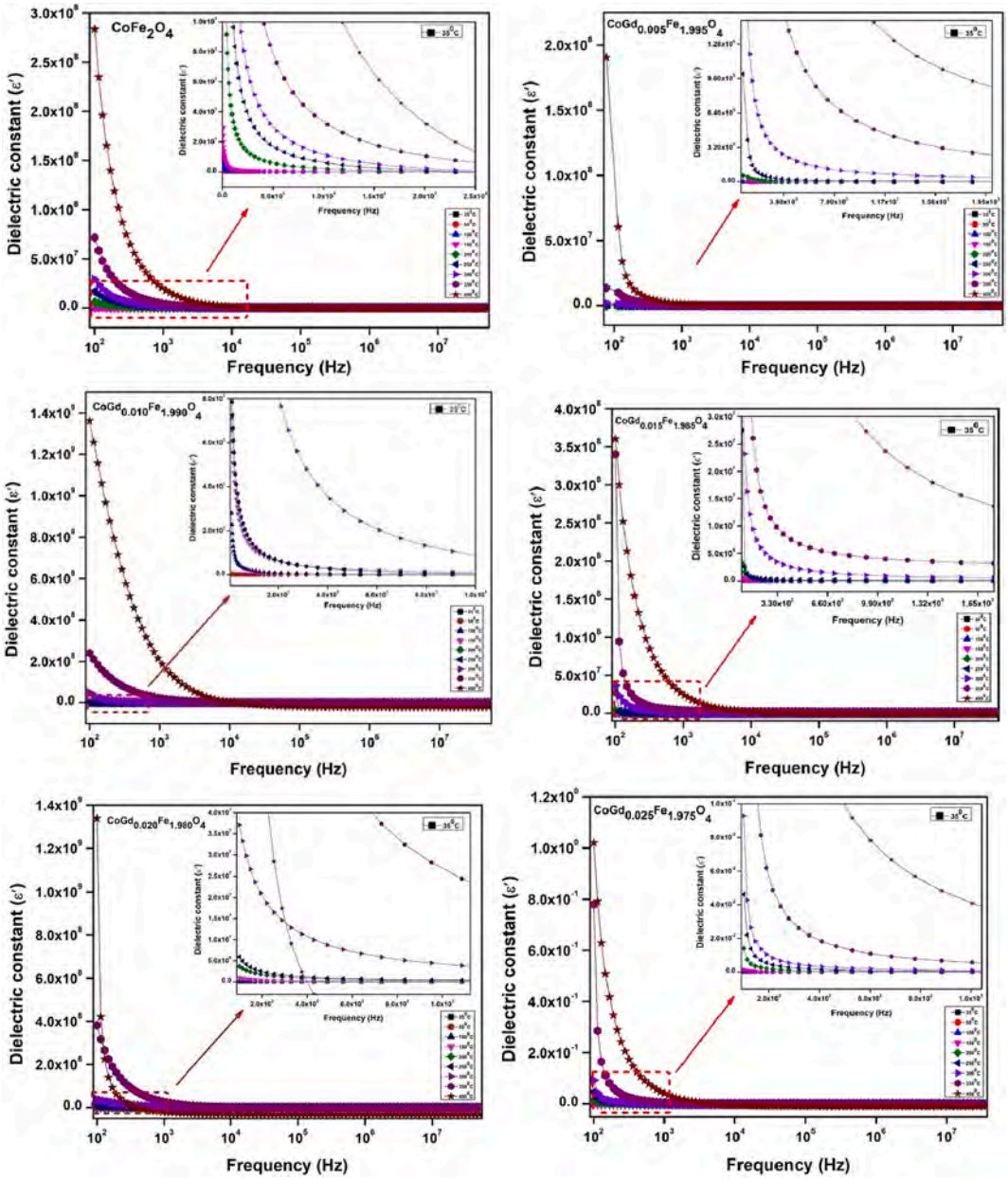

Fig. 8. (a-f). Variation of Dielectric constant (ε′) of $CoGd_xFe_{2-x}O_4$ (x = 0–0.025 in an interval of 0.005) ferrites as a function of frequency.

where $\left(\frac{K\lambda}{Dcos\theta}\right)$ **is** broadening due to the size (D) and 4εtanθ is broadening due to strain (ε)[16,17]. After modification of above equation yields, i.e.,

$$\beta cos\theta = \frac{0.9\lambda}{D} + 4\varepsilon sin\theta \quad (7)$$

Figure 3 depicts the W-H plots of the prepared samples, whereas Figure 4 depicts the change in crystalline size and microstrain with regard to composition. An rise in XRD can be caused by a variety of additional factors, including roughness, dislocations, strain, and crystallite size. The XRD peak position may shift as a result of the employment of dopants, however this shift is not always predictable and can rely on a number of variables, including the size of the dopant and the crystalline structure of the material.

3.2. SEM and EDAX analysis

Figure 5 depicts SEM micrograph images of CGF (x = 0–0.025 in intervals of 0.005) nanoferrite samples. Particle aggregation can be seen vividly in SEM micrographs. Particles are homogenous, evenly dispersed, and somewhat agglomerated, according to the photos. This aggregation could be owing to magnetic interactions or an enhanced surface-to-volume ratio [19–21]. For CGF materials, the results nano meter ranged, it was discovered. The average crystal size ascertained using XRD shows good agreement with SEM pictures [22].

The EDAX spectrum quantitatively confirms the purity of the synthesised ferrites, as well as the presence of Co, Fe, and O in the pure sample and Gd in doped samples [23,24]. The EDAX spectrum of CGF (x = 0–0.025 in an interval of 0.005) nanoferrite is displayed in Figure 6 and corresponds to the SEM micrographs and data in Table 2. SEM and EDX have both been used to examine the morphology and chemical makeup of every product [25].

3.3. Dielectric studies

The dielectric investigations shed light on the material's method of

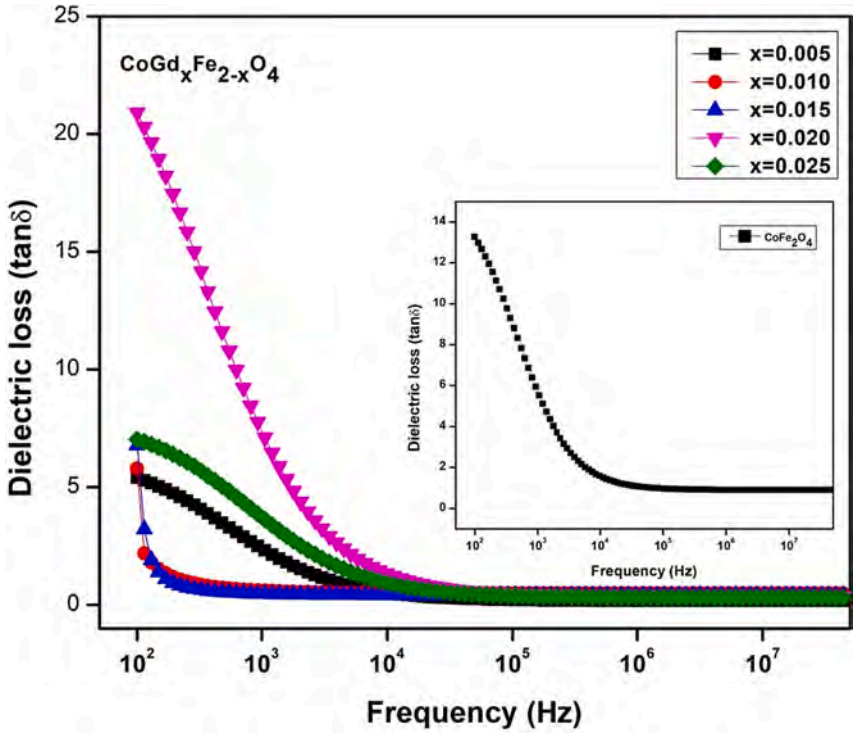

Fig. 9. Variation of Dielectric loss (tanδ) of $CoGd_xFe_{2-x}O_4$ samples (x = 0.0—0.025) as a function of frequency at room temperature.

electric conduction. In order to study the dielectric properties of gadolinium-doped cobalt ferrites, a Bode 100 impedance analyzer with a frequency range of 50 Hz to 5 MHz is used at room temperature as well as between 30 °C and 500 °C. Utilising the formula [26], the values of the dielectric constant with applied frequency are determined.

$$\varepsilon\varepsilon' = \frac{ccd}{\varepsilon\varepsilon_\circ AA} \tag{8}$$

Where A is the cross-sectional area of the pellet, d is its thickness, $\varepsilon_\circ$ is its permittivity, and C is its capacitance.

3.3.1. Variation in the dielectric constant (ε') with frequency

Figures 7 (at 30 °C) and 8 (a-f) (from 35 °C to 400 °C) show the frequency dependence of the dielectric constant for CGF (x = 0–0.025 in an interval of 0.005) ferrites. The figure shows that the measured value of the dielectric constant substantially varies with the frequency of the applied field. The figure clearly shows that the dielectric constant declines as frequency rises and that it does so abruptly in the low frequency zone (up to 1 kHz) before tending to be frequency independent in the high frequency region (10 kHz). Consequently, it exhibits dispersion behaviour at low frequencies. According to Koop's phenomenological theory [27,28], this variation in the dielectric constants can be attributed to the Maxwell-Wagner type of interfacial polarisation. This indicates that there are two conducting layers in the dielectric medium. Large grains in the first layer act as well-conducting grains, but grain boundaries in the second layer exhibit low conductivity. Polarisation in ferrites is a mechanism akin to the conduction process. Due to the grain borders' greater resistance and the subsequent charge accumulation there due to electron and hole hopping between Co^{2+} and Fe^{2+} and Co^{2+} and Co^{3+} ions, interfacial polarisation is created.

Although the charge carriers were unable to follow the applied field as its frequency increased, this resulted in a decrease in polarisation [29]. According to figure 7, the dielectric constant also rises in cobalt ferrite with an increase in Gd^{3+}, with the exception of X = 0.020, where it reaches its maximum. Cobalt ferrite literature [30–32] likewise reported an identical outcome. Figure 8 shows that $CoGd_{0.025}Fe_{1.975}O_4$ has a lower 32-dielectric constant than $CoGd_{0.020}Fe_{1.980}O_4$. This may be because the increased Gd^{3+} concentration was not incorporated into the cobalt ferrite, which results in a lower dielectric constant [33].

3.3.2. Variation in the dielectric loss (tanδ) with frequency

A measurement of polarisation lag in relation to an alternating field is the dielectric loss. Figures 9 (at 30 °C) and 10 (a-f) (from 35 °C to 400 °C) show the frequency-dependent dielectric loss (tanδ) for CGF (x = 0–0.025 in an interval of 0.005) ferrites. The figure shows that, at low frequencies, the dielectric loss decreases with increasing frequency while becoming independent at higher frequencies, which is consistent with the behaviour of ferrites. Substantial resistance at the grain boundary is typically associated with low-frequency regions; as a result, the largest amount of energy is needed in these regions for the exchange of electrons between Fe2 + and Fe3 + ions, leading to substantial loss. (See Fig 10).

In the case of high frequency, there is less energy. Higher frequencies hence exhibit a lower degree of dielectric loss, which is suitable for high-frequency device applications.

3.4. AC conductivity

The fluctuation in AC conductivity as a function of frequency has been investigated in order to better understand the conduction process and the hopping of charge carriers that affect it. Using the relation, ac conductivity was computed.

$$\sigma = 2\pi f \varepsilon_\circ \varepsilon' \tan\delta \tag{9}$$

Fig 11 (a–f) illustrates how the conductivity rises as the frequency rises. The low-frequency conductivity of Ac is roughly linear or frequency-dependent, indicating that a small polaron is responsible for the conduction. Electron and hole hopping between Co^{2+} and Co^{3+} in octahedral sites is the primary cause of conduction in ferrites. The Maxwell-Wagner model [27], which was previously mentioned, can also be used to explain how the conductivity of Ac varies with frequency. At low frequencies, high-resistance grain boundaries become more active,

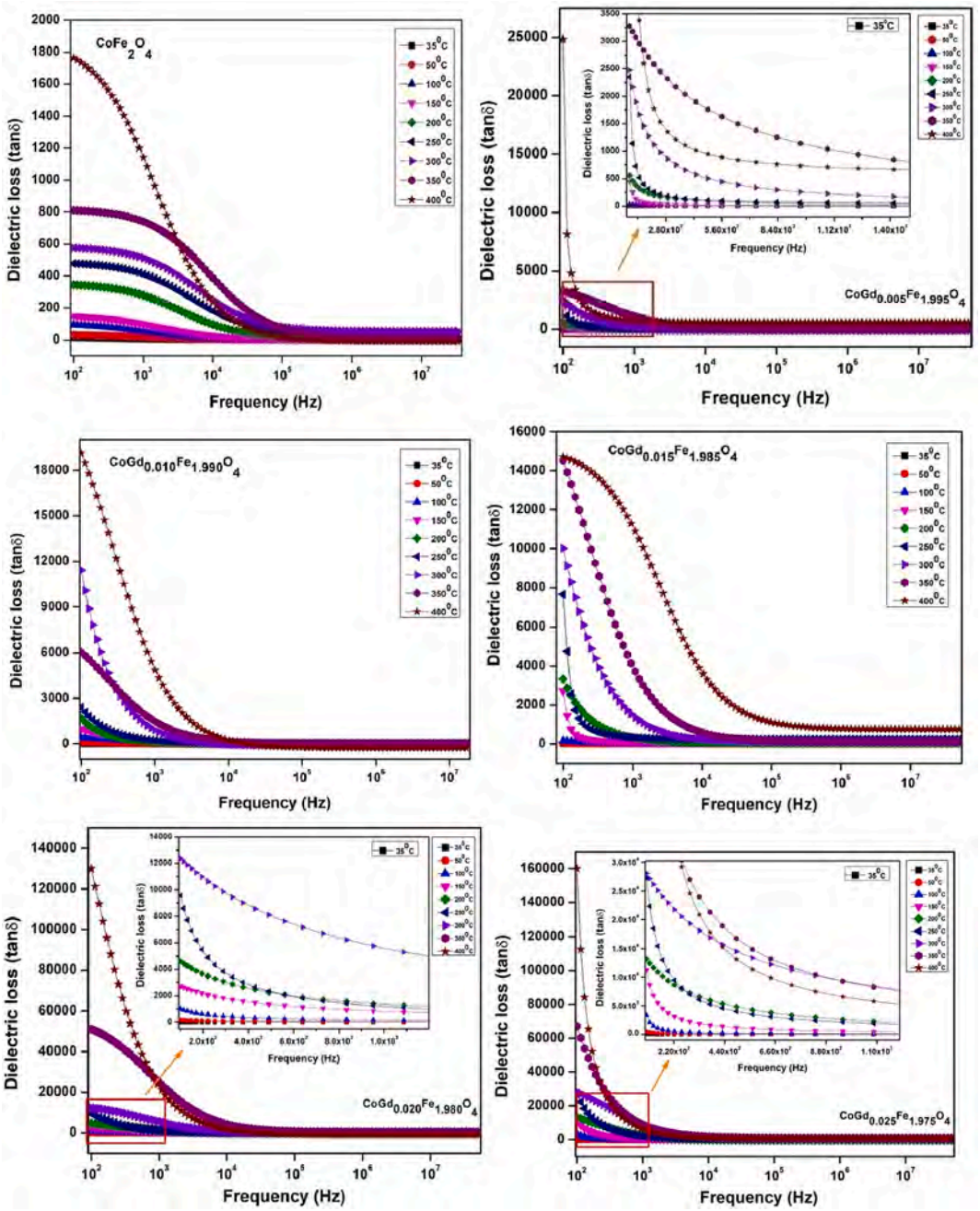

Fig. 10. (a-f). Variation of Dielectric loss (tanδ) of $CoGd_xFe_{2-x}O_4$ samples (x = 0.0—0.025) as a function of frequency.

which prevents electrons from hopping between Fe^{3+} and Fe^{2+} cations. Ac conductivity decreases as a result. When an alternating field's frequency is increased, conducting grains become active, and the interchange of electrons between the Fe^{3+} and Fe^{2+} cations increases. As hopping increases, ac conductivity rises. It is possible to alter the conduction mechanism by changing the Gd^{3+}-ion substitution [34–36].

Additionally, it is evident from Table 3 that the produced ferrites' frequency-dependent Ac conductivity is significantly influenced by the Gd^{3+} content. With the exception of x = 0.020, all conductivity readings as a function of frequency demonstrate an increase in conductivity with rising Gd concentration. The dielectric constant of ferrite materials is governed by the conduction process. The relationship between the AC conductivity and the dielectric constant and loss can be seen in the equation $\sigma = 2\pi f \varepsilon_\circ \varepsilon' \tan\delta$,. The amount of Fe^{2+} or Fe^{3+} cations present at octahedral B sites in ferrites controls the dielectric constant.

Because Gd ions are substituted for Fe ions in substations, which lower the amount of Fe ions at the A-site, Fe ions from the A-site go towards the B-site. Decreased polarisation or a rise in the dielectric constant will result from an increase in the electron transfer between Fe^{3+} and Fe^{2+} ions [37,38]. As both depend on and are proportional to the number of Fe ions present at the octahedral B site, the increasing trend in Ac conductivity following Gd doping is also reflected in the dielectric constant. However, the behaviour of the frequency-dependent dielectric constant and the AC conductivity varies at lower and higher frequencies. As can be shown, the octahedral B site conductivity and frequency have a direct relationship, but the dielectric constant has an inverse relationship to frequency [39]. The dielectric parameters such as dielectric constant, dielectric loss, and AC conductivity at room temperature are listed in Table 3.

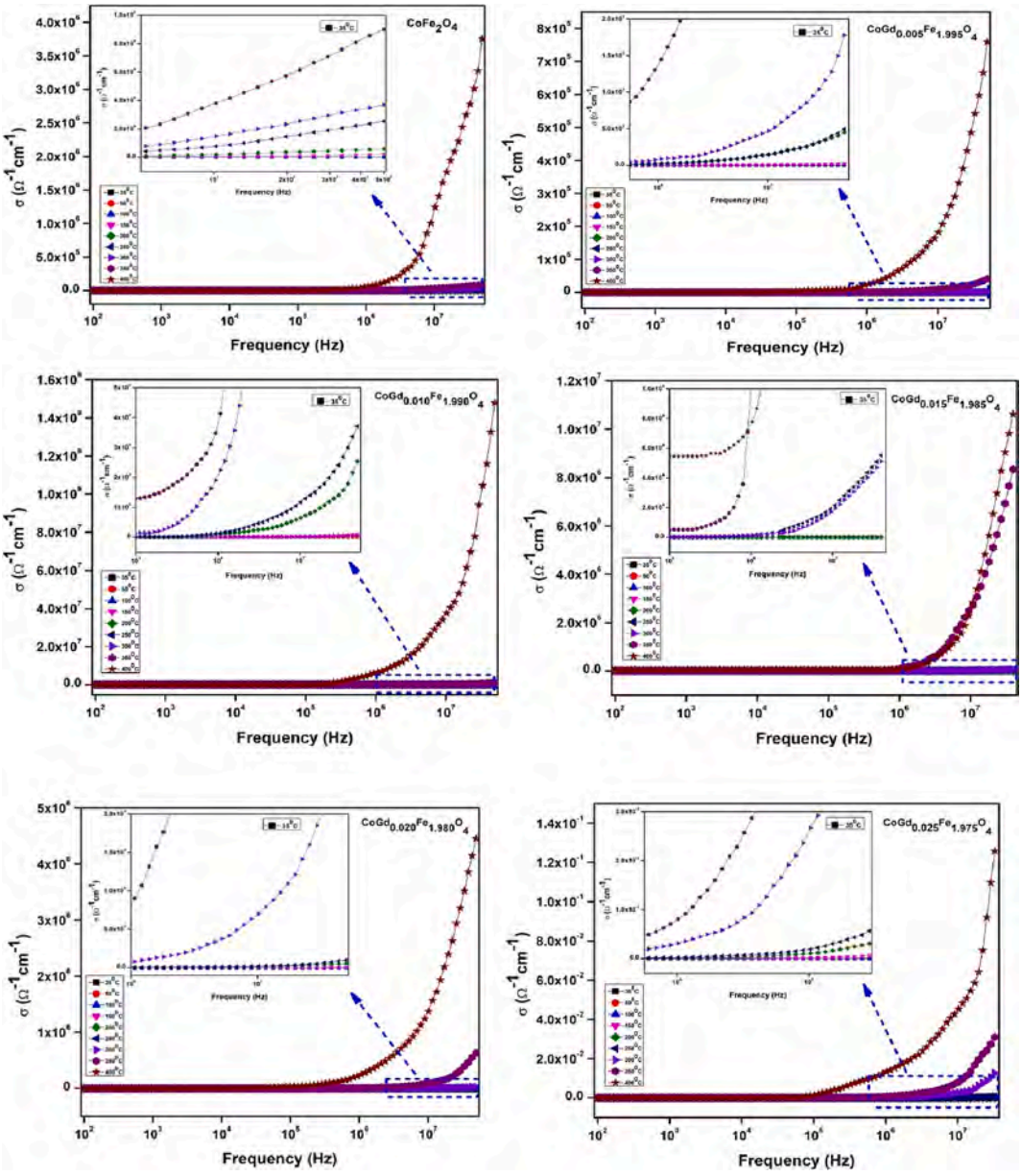

Fig. 11. (a-f). Variation of Ac conductivity of $CoGd_xFe_{2-x}O_4$ samples (x = 0.0—0.025) as a function of frequency.

Table 3
ε', tanδ and σ values at room temperature of $CoGd_xFe_{2-x}O_4$ (x = 0–0.025 in an interval of 0.005) nanoferrites.

composition	ε'		tanδ		σ (Ω^{-1}-Cm^{-1})	
	100 Hz	1KHz	100 Hz	1KHz	100 Hz	1KHz
0	349.1794	12.49073	13.26834	1.49265	3.22E-05	8.38E-06
0.005	10.66047	0.20638	5.39722	0.47744	1.08E-06	4.60E-08
0.010	12.03766	0.25001	5.78852	0.51106	6.98E-07	1.87E-08
0.015	15.97785	0.28418	6.78691	0.60432	9.75E-07	3.15E-08
0.020	58.96164	2.53163	20.91408	1.2278	1.73E-05	1.77E-06
0.025	35.28428	1.20314	7.03561	0.86583	2.46E-09	1.97E-09

4. Conclusions

The gadolinium-doped cobalt ferrite samples were studied. The X-ray diffraction powder patterns were used to confirm phase identification and spinel structure, and the Williamson-Hall plot was used to investigate the crystalline size and lattice strain on the peak broadening of each sample, with crystalline size ranging from 13 to 48 nm. Particle aggregation can be seen vividly in SEM micrographs, and the EDAX spectrum quantitatively confirms the purity of the synthesised ferrites. At low frequencies, high-resistance grain boundaries become more active, which prevents electrons from hopping between Fe^{3+} and Fe^{2+} cations. Ac conductivity decreases as a result.

Declaration of competing interest

The authors declare that they have no known competing financial interests or personal relationships that could have appeared to influence the work reported in this paper.

Data availability

The data that has been used is confidential.

Acknowledgement

The authors are thankful to SVS, Head and BOS, Department of Physics, Osmania University for his support.

References

[1] Shinde A. B, Structural and electrical properties of cobalt ferrite nanoparticles. Int J Innov Technol Explor Eng. 3 (2013) 64-7.
[2] Shirsath S.E, Wang D, Jadhav S.S, Mane M.L, Li S, Ferrites Obtained by Sol-Gel Method. In: Klein, L., Aparicio, M., Jitianu, A. (eds) Handbook of Sol-Gel Science and Technology. Springer, Cham (2018).
[3] M.Y. Chen, J. Xu, Z.Z. Li, Y. Zhang, W.H. Qi, G.D. Tang, Magnetic property and cation distributions in boron-doped MFe2O4(M = Ni, Mn) spinel ferrites, Results Phys. 14 (2019), 102389.
[4] AMM Farea, S Kumar, KM Batoo, A Yousef, CG Lee Structure and electrical properties of $Co_{0.5}Cd_xFe_{2.5-x}O_4$ ferrites Journal of Alloys and Compounds 464 (1-2), 361-369.
[5] S. Munir, M.F. Warsi, S. Zulfiqar, I. Ayman, S. Haider, I.A. Alsafari, P.O. Agboola, I. Shakir, Nickel ferrite/zinc oxide nanocomposite: Investigating the photocatalytic and antibacterial properties, J. Saudi Chem. Soc. 25 (2021), 101388.
[6] AMM Farea, S Kumar, KM Batoo, A Yousef Influence of frequency, temperature and composition on electrical properties of polycrystalline $Co_{0.5}Cd_xFe_{2.5-x}O_4$ ferrites Physica B: Condensed Matter 403 (4), 684-701.
[7] M.A. Almessiere, B. Unal, A. Demir Korkmaz, A. Baykal, Y. Slimani, M.A. Gondal, U. Baig, A.V. Trukhanov, Electrical and dielectric property of rare earth substituted hard-soft ferrite (Co0.5Ni0.5Ga0.01Gd0.01Fe1.98O4)x/(ZnFe2O4)y nanocomposites, J. Mater. Res. Technol. 15 (2021) 969–983.
[8] Mohd. Hashim, M. Raghasudha, Sher Singh Meena, Jyoti Shah, Sagar E. Shirsath, Shalendra Kumar, D. Ravinder, Pramod Bhatt, Alimuddin, Ravi Kumar, R.K. Kotnala, Influence of rare earth ion doping (Ce and Dy) on electrical and magnetic properties of cobalt ferrites, Journal of Magnetism and Magnetic Materials 449 (2018) 319–327, https://doi.org/10.1016/j.jmmm.2017.10.023.
[9] Arvind Kumar,Mahendra Kumar Gora, Sanjay Kumar, Banwari Lal Choudhary, Rishi Kumar Singhal, Satya Narain Dolia, Study of electronic structure and dielectric properties of Gd–doped cobalt nanoferrites, Journal of the Korean Physical Society (2022) 81:894–902, https://doi.org/10.1007/s40042-022-00612-w.
[10] C. Murugesan, G. Chandrasekaran, Impact of Gd3+-substitution on the structural, magnetic and electrical properties of cobalt ferrite nanoparticles, RSC Adv. 5 (2015) 73714–73725.
[11] Erum Pervaiz and I H Gul, Influence of Rare Earth (Gd^{3+}) on Structural, Gigahertz Dielectric and Magnetic Studies of Cobalt ferrite, Journal of Physics: Conference Series 439 (2013) 012015, doi:10.1088/1742-6596/439/1/012015.
[12] M. Kamran, M. Anis-ur-Rehman, Influence of La3+ substitutions on structural, dielectric and electrical properties of spinel cobalt ferrite, Ceram. Int. 49 (2023) 7017–7029, https://doi.org/10.1016/j.ceramint.2022.10.127.
[13] L. Avazpour, H. Shokrollahi, M.R. Toroghinejad, M.A. Zandi Khajeh, Effect of rare earth substitution on magnetic and structural properties of Co1−xREx Fe2O4 (RE: Nd, Eu) nanoparticles prepared via EDTA/EG assisted sol–gel synthesis, J. Alloys Compd. 662 (2016) 441–447.
[14] Yuzheng Lu, Muhammad Yousaf b , Majid Niaz Akhtar, Asma Noor, Muhammad Akbar, M.A.K. Yousaf Shah, Senlin Yan, Faze Wang, Effect of Gd and Co contents on the microstructural, magneto-optical and electrical characteristics of cobalt ferrite (CoFe2O4) nanoparticles. https://doi.org/10.1016/j.ceramint.2021.10.067.
[15] Shantha kumari, N. Hari Kumar, Avula Edukondalu, D. Ravinder Effect of Neodymium Doping on Structural, Optical and Dielectric Properties of Ni Ferrites Synthesized by Citrate gel Auto-combustion Method 34.25 (2023)10 10.1007/s10854-023-11193-0.
[16] V. Ludhiya, N. Hari Kumar, Avula Edukondalu, D. Ravinder, Solution combustion synthesis of nanostructured $Mg_{0.5}Ni_{0.3}Cu_{0.2}Ce_xFe_{2-x}O_4$ ferrites: structural, optical and electromagnetic properties. Applied physics A 129 (9), 614 (2023).
[17] M.A. Almessiere, Y. Slimani, M. Sertkol, H. Gungunes, Y.S. Wudil, A. Demir Korkmaz, A. Baykal, Impact of Gd substitution on the structure, hyperfine interactions, and magnetic properties of Sr hexaferrites, Ceram. Int. 47 (2021) 33853.
[18] Banoth Baburao, N. Hari kumar, Avula Edukondalu, M. Venkata Narayana, D. Ravinder, Structural, optical, DC electrical, thermo-electric, dielectric and magnetic properties of $Mg_{0.8}Zn_{0.2}Gd_xFe_{2-x}O_4$ nanoparticles synthesised by citrate-gel auto combustion method, Inorg. Chem. Commun. 148 (2023) 110355. https://doi.org/10.1016/j.inoche.2022.110355.
[19] Y. Slimani, M.A. Almessiere, A. Demir Korkmaz, A. Baykal, M.A. Gondal, H. Güngüneş, S.E. Shirsath, A. Manikandan, Investigation of the structural, morphological, and magnetic properties of (Ni0.5Co0.5)[GaxGdxFe2-2x]O4 nanoparticles prepared via sonochemical approach, J. Rare Earth 41 (2023) 561.
[20] N.d. Alfryyan, S. Munir, Z.A. Muqadas Latif, M.-B. Alrowaili, A. Irshad, M. Suleman, Synthesis of CNT supported nickel and cobalt doped zinc ferrite for photodegradation of organic effluents by visible light irradiation, Optik 228 (2023), 171213.
[21] B. Aparna, N. Hari kumar, A. Edukondalu, D. Ravinder, K.A. Jaleeli, P-type semiconductor Gd/Fe ion doped Ni-Mg nanoferrites applications, Results in Chemistry 5 (2023) 100957.
[22] B Suryanarayana, KLV Nagasree, PSV Shanmukhi, MG Kiran, N Murali et.al, Effect of Cu^{2+}/Ce^{3+} substituted on synthesis, structural, morphological, magnetic, DC electrical resistivity and dielectric properties of Cobalt nano ferrites (2023) doi.org/10.21203/rs.3.rs-3371511/v1.
[23] V Jagadeesha Angadi, KM Batoo, S Hussain, SO Manjunatha, S Wang et.al, Synthesis and study of transition metal (Co, Cu, and Ni) substituted ferrites for humidity sensor applications Journal of Materials Science: Materials in Electronics 34 (4), 301.
[24] Y. Slimani, M.A. Almessiere, A. Demir Korkmaz, A. Baykal, A. Manikandan, H. Gungunes, M.S. Toprak, Ultrasound synthesis and magnetic investigations of Ni0.4Cu0.4Zn0.2GaxGdxFe2-2xO4 (x ≤ 0.04) nanospinel ferrites, Appl. Phys. A 128 (2022) 593.
[25] R. Quhe, J. Zheng, G. Luo, Q. Liu, R. Qin, J. Zhou, D. Yu, S. Nagase, W.N. Mei, Z. Gao, J. Lu, Tunable and sizable band gap of single-layer graphene sandwiched between hexagonal boron nitride, NPG Asia Mater. 4 (2012), https://doi.org/10.1038/am.2012.10.
[26] KM Batoo, M Hadi, A Chauhan, R Verma, M Singh, OM Aldossary et. al, High-frequency applications of bismuth-doped Co-Zn ferrite nanoparticles for electromagnetic interference filter and multilayer inductor chip fabrication Applied Physics A 128 (4), 283.
[27] M.A. Unal, A. Almessiere, Y. Baykal, A. Slimani, Sadaqat, Anwar UI-Hamid, A study on the electrical and dielectric traits of ternary NiCuZn-spinel ferrites co-substituted with Ga3+-Gd3+ ions, Mater. Sci. Eng. B 289 (2023), 116429.
[28] W.R. Agami, Effect of neodymium substitution on the electric and dielectric properties of Mn-Ni-Zn ferrite, Phys. B Condens. Matter. 534 (2018) 17–21, https://doi.org/10.1016/j.physb.2018.01.021.
[29] J. C. Maxwell, A Treatise on Electricity and Magnetism, Oxford University Press, London, 1973 Search PubMed.
[30] C. G. Koops, On the dispersion of resistivity and dielectric constant of some semiconductors at audiofrequencies Phys. Rev., 1951, 83, 121 CrossRef CAS.
[31] Banoth Baburao, N. Hari Kumar, Avula Edukondalu, D. Ravinder, Influence of Er/Fe substitution on Mg-Zn nanoparticles' electromagnetic properties and applications, Braz. J. Phys. 53 (91) (2023) 1–15.
[32] B. Debnath, S. Parvin, H. Dixit, S. Bhattacharyya, ChemSusChem 15 (2020) 3875–3886, https://doi.org/10.1002/cssc.202000932.
[33] F.R. Mariosi, J. Venturini, A.C. Viegas, C.P. Bergmann, Ceram. Int. 46 (3) (2020) 2772–2779, https://doi.org/10.1016/j.ceramint. 2019.09.266.
[34] N. Sivakumar, A. Narayanasamy, C.N. Chinnasamy, B. Jeyadevan, J. Phys.: Condens. Matter 19 (2007), 386201.
[35] N. Hari Kumar, A. Edukondalu, D. Ravinder, Structural, dielectric, and magnetic properties of Cu-doped Ni-Zn ferrites, J. Aust. Ceram. Soc. 1–15 (2023).
[36] B. Unal, M.A. Almessiere, Y. Slimani, et al., A study on the electrical and dielectric properties of SrGdxFe12−xO19 (x = 0.00–0.05) nanosized M-type hexagonal ferrites, J. Mater. Sci.: Mater. Electron. 32 (2021) 18317–18329, https://doi.org/10.1007/s10854-021-06373-9.
[37] SR Kumar, GV Priya, B Aruna, MK Raju, D Parajuli, N Murali, R Verma et.al, Influence of Nd^{3+} substituted $Co_{0.5}Ni_{0.5}Fe_2O_4$ ferrite on structural, morphological, dc electrical resistivity and magnetic properties Inorganic Chemistry Communications 136, 109132.
[38] M.T. Rahman, C.V. Ramana, Impedance spectroscopic characterization of gadolinium substituted cobalt ferrite ceramics, J. Appl. Phys. 116 (16) (2014 Oct 28), 164108.
[39] N. Hari kumar, D. Ravinder, T. AnilBabu, Nakiraboina Venkatesh, S. Swathi, N. V. Krishna Prasad, Development of Cu^{2+} substituted Ni-Zn ferrite nano-particles and their high-temperature semiconductor behaviour. Journal of Indian chemical society 99 (2022) 100362. https://doi.org/10.1016/j.jics.2022.100362.